ORIGINAL ARTICLE

Effect of Surface Preparation on the Air Oxidation Behaviour of Modified 9Cr–1Mo Steel

Ch. Jagadeeswara Rao[1] · **M. Archana[1]** · **S. Ningshen[1]**

Abstract Air oxidation behaviour of modified 9Cr–1Mo steel with different surface treatments is evaluated at 650 °C for about 100 h. Modified 9Cr–1Mo steel with four different surface treatments, i.e. grit blasting, grinding (120 grit finish and 600 grit finish) and diamond finish (mirror polishing), was studied to ascertain the effect of surface preparation on oxidation behaviour. The grit-blasted sample exhibited more weight gain compared to other samples, and the weight gain was higher during the initial oxidation. The nature and formation of oxide crystals/oxide layer across the surface were visualized by SEM analysis. The formation of Cr- and Fe-rich oxides on the surface, and Cr-based oxides at the interface were confirmed by the Raman spectroscopy and GDOES analysis. The formation of $MnCr_2O_4$ was also evidenced. The oxide layer thickness was measured using GDOES-DiP technique.

Keywords Modified 9Cr–1Mo steel · Oxidation · Surface treatments · Glow discharge optical emission spectrometry

1 Introduction

The 9Cr–1Mo steels are being used as candidate materials for the construction of various components for high temperature applications. It is also used for the manufacturing of steam generator components in the Prototype fast breeder reactor (PFBR), which is under the final stage of commissioning at Kalpakkam, India [1–3]. Chromoly steels, especially 9Cr–1Mo, are used as construction materials of various parts in power plants due to their desirable mechanical stability, corrosion resistance in air and steam environments [1]. Especially, the modified 9Cr–1Mo steel with the addition of Vanadium (V) and Niobium (Nb) is chosen for the steam side applications in the PFBR with enhanced high temperature mechanical properties of the alloy. The PFBR steam generator is a shell and tube type heat exchanger, sodium flows in the shell side, and water flows in the tube side of the exchanger. Hence, the steam generator component's performance during the service should not lead to the contact of sodium with water, which will result in a violent reaction. Thereby, materials for the steam generator applications require high oxidation resistance in both steam and air at high temperatures, creep and low cycle fatigue resistance, etc. [2, 4].

The air and steam oxidation behavior of the alloys are very vital for their applications in different environments, like, in the atmospheric air, steam, etc. at high temperature. The oxidation of the alloys at high temperature needs to be understood before choosing the materials for such applications. The nature and stability of oxide films and the kinetics of oxidation would suggest the corrosion resistance of the material for high temperature applications. Generally, oxidation could lead to the loss of underneath alloy, which impacts the service life of the alloy under loads, if any, during the service. The corrosion resistance of the metal/alloy would be increased if the metal/alloy forms a stable thick oxide film with good properties. Generally, the oxide films should possess good adherence, high melting point, low vapour pressure, etc. for protecting the underneath alloy at high temperature applications from further oxidation. Hence, it is essential to study the oxidation resistance of these high temperature alloys for their use as structural materials.

✉ Ch. Jagadeeswara Rao
cjrao@igcar.gov.in; chowdarij@gmail.com

[1] Corrosion Science and Technology Division, Metallurgy and Materials Group, Indira Gandhi Centre for Atomic Research, A CI of Homi Bhabha National Institute, Kalpakkam, Tamilnadu, India

Several studies on the oxidation of Chromoly steels and especially about 9Cr–1Mo steel in high temperatures in various environments are reported. There are some studies about the 2.25Cr–1Mo steel in various conditions reported [5–7]. These studies on 2.25Cr–1Mo steel indicated the formation of layered structure oxide scale during oxidation in dry oxygen at 600 °C and above. The oxide scales mostly comprised of inner doped spinel, intermediated magnetite and the outer hematite layer [6, 7]. The 90% cold work of the alloy led to the formation of Cr-rich spinel and slowed down the oxidation of the alloy at above 700 °C [5]. The oxidation behaviour of 9Cr–1Mo steel was also investigated in different environments. Most of the reports about the oxidation of Fe-based alloys at high temperature in air revealed the formation of duplex oxides containing Fe-rich oxides on top and Fe and Cr spinels at the oxide-alloy interface. Recently, the authors showed the use of glow discharge optical emission spectrometer for the characterization of oxidized modified 9Cr–1Mo steel samples and found out the variation of oxides nature across the thickness of the oxide layer with the duration of oxidation [8].

Most of the reported studies on alloys and especially on 9Cr–1Mo steel are carried out on ground/polished samples, where the surface finish is smooth. However, in real applications as structural materials for the components at high temperature, the samples will be in machined finish or with some surface activated finish. The surface finish of the material will also affect the oxidation resistance of the material, which in turn changes the life expectancy of the material in service [9–13]. Surface finish plays a decisive role in the oxidation behaviour of alloys at high temperatures [14]. There are handful studies on the effect of surface preparations on oxidation behaviour reported in the literature. Rai et al. [10] studied the effect of laser shock peening on the oxidation behaviour of modified 9Cr–1Mo steel at temperatures between 600–700 °C, and reported the enhancement of oxidation resistance of the material after laser shock peening. Nowak et al. [15] reported the effect of surface mechanical treatment on the oxidation of FeAl model alloy, and the results revealed the influence of surface treatment on the oxidation kinetics and oxide scale microstructures of alloy. Platt et al. [13] studied the effect of surface roughness on Zircaloy-4 oxidation in steam at 400 °C and reported well-defined changes in the oxidation kinetics with respect to surface roughness of the samples. Cheng et al. [16] reported the two different oxidation models observed during the oxidation of nickel-based super alloys, DD6 and DZ125,

at 950 °C with various initial surface roughness. Xia et al. [12] reported a three layered oxide formation on nanocrystalline surface layered P91 steel during oxidation in water vapour. The three layers consisted of Fe_3O_4, spinel $FeCr_2O_4$ and $(Fe,Cr)_2O_3$ from top surface of oxide, respectively. The effect of surface roughness of AISI 316Ti stainless steel on the oxidation kinetics was studied by cyclic oxidation tests at 900 and 1000 °C [9]. Ghosh et al. [17] studied the oxidation behaviour of 304L stainless steel in machined, ground and solution annealed conditions at 300 °C in water. They reported the dependency of surface working on the morphology and nature of oxides and thick oxide scales found in case of solution annealed condition compared to other conditions. Das et. al. [18] studied in detail the effect of various surface treatments on the high temperature high pressure oxidation of type 304L stainless steel in water and reported that the diamond finish sample had more thicker oxide scale than other surface finishes and the electropolished surface showed more protective oxide than the other finished surfaces like the diamond finish, 600 grit finish and machined.

Most of the studies indicated the effect of roughness/surface preparation on the oxidation behaviour of the materials at high temperatures. The present study focused on the effect of surface roughness created by mechanical treatments, grit blasting, ground and polishing on modified 9Cr-1Mo steel for air oxidation at 650 °C for about 100 h.

2 Experimental Procedure

2.1 Oxidation Tests

Table 1 provides the composition of the modified 9Cr–1Mo steel sample analysed by inductively coupled plasma-optical emission spectroscopy (ICP-OES). The modified 9Cr–1Mo test samples of size 25 mm (L) × 25 mm (W) × 5 mm (thickness) were out from a plate. Four different surface finished samples were used in the present study and were designated as grit blasted (sample No.1), ground successively up to 120 SiC abrasive paper (sample No.2), ground successively up to 600 abrasive paper (sample No.3), and polished up to diamond finish (sample No.4) using 0.5 µm diamond paste. All the samples were surface prepared on all sides. Grit blasting was done on all sides of the sample by using 16 mesh alumina grit at a blasting air pressure of 3 bar(g) in a pressure blasting unit (M/s. Metallizing Equipment Co.Pvt. Ltd. India). All the specimens were cleaned using water and

Table 1 The elemental composition of modified 9Cr–1Mo steel

Composition (wt%)	C	Cr	Mo	Si	Mn	V	Nb	Ni	Fe
Modified 9Cr–1Mo steel	0.104	8.97	0.94	0.41	0.55	0.20	0.09	0.20	Balance

ethanol by ultrasonication after surface preparations and dried in the air before carrying out air oxidation studies. The surface areas of the four samples were measured from the dimensions and the surface areas were 34.03, 18.08, 17.64 and 18.19 cm^2 for grit blasted, 120 grit finish, 600 grit finish and diamond finish samples, respectively. The surface profiles of the samples before and after the oxidation test were measured by a profilometer (Talysurf CLI 1000, M/s. Taylor Hobson). Weights of the samples before and after the oxidation test were measured using an ultra-microbalance (XPE 26, M/s. Mettler Toledo) with 1 µg readability.

The air oxidation tests were carried out in a vertical tubular furnace under ambient air atmosphere. The experimental set-up is shown in Fig. 1. All the samples were kept in an alumina crucible. The alumina crucible was baked for about 10 h at 650 °C to avoid any moisture before placing the samples. Once the furnace temperature reached 650 °C, the samples were directly placed in the alumina crucible kept in the furnace. The temperature of the samples was measured using K-type thermocouple attached to dummy sample kept along with the test samples. During the entire oxidation duration, the room temperature was between 20–25 °C with a relative humidity of 80–90%. The air oxidation studies were repeated twice for two sets of samples.

2.2 Characterization Tools

Laser Raman spectroscopic analysis (LRS) was carried out using Raman spectrometer (HR800, M/s. Jobin Yvon), using He–Ne laser ($\lambda = 633$ nm) and 1800 gr/mm holographic grating with the analysis spot size of 3 µm. The surface morphology of the oxides was obtained by FESEM (SUPRA 55 Zeiss). The Glow discharge optical emission spectrometric (GDOES) analysis was carried out using GDOES profiler-2 (M/s. Horiba Jobin Yvon, France) along with DiP

Fig. 1 Schematic of the experimental setup

(differential interferometry profiling) system. The analysis of the oxide layers along the thickness of the film was characterized by DiP technique. Suitable wavelengths of emission lines of various elements, like Cr (425.439 nm), Fe (371.999 nm), Mn (403.455 nm), Mo (386.416 nm), and O (130.233 nm), were used in order to elude overlaps of various elements emission lines. All the DiP measurements were carried out using radio frequency (RF) excitation mode with the following plasma conditions; DiP anode size: 4 mm, argon gas pressure: 750 Pa, Power: 35 W, DiP gain: 100, flush time: 70 s. The intensities of the elements, O and Mn were multiplied by a factor of 5 and plotted in Figs. 9 and 10.

3 Results and Discussion

3.1 Evaluation of Surface Roughness

Table 2 provides the parameters obtained from surface roughness profiles of the samples before oxidation test. R_a is the arithmetic mean deviation of the roughness profile, R_q is the root-mean-square (RMS) deviation of the roughness profile, R_p is the maximum peak height of the roughness profile, R_v is the maximum valley depth of the roughness profile and R_z is the maximum height of roughness profile.

The values of the parameters for various surface finish samples indicate that the extent of surface roughness increases with polishing, grinding and grit blasting. The diamond finish sample shows the smoothest surface compared to other samples. The grit-blasted sample shows the more rough surface among all the samples.

3.2 Oxidation Kinetics

The plot of change in weight per surface area of modified 9Cr–1Mo steel versus the duration of oxidation is shown in Fig. 2. The grit-blasted samples show more weight gain compared to other surface finish samples per unit surface area. The weight of the grit-blasted sample shows increasing pattern from initial period to the next period 25 h and, then, up to 100 h, and the weight gain of the grit-blasted sample is higher in the initial periods of oxidation compared to the final stage of oxidation. The weight gain for
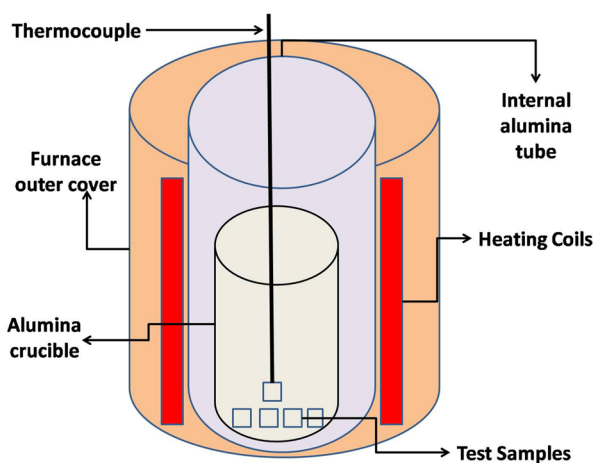
Table 2 The surface roughness parameters of the samples

Sample type	Diamond finish	600 Grit	120 Grit	Grit blasted
R_a in µm	0.0103 ± 0.002	2.23 ± 0.4	2.62 ± 0.5	8.99 ± 2
R_q in µm	0.0136	2.88	3.21	10.85
R_p in µm	0.00961	5.74	6.46	22.01
R_v in µm	0.0187	5.58	6.52	23.82
R_z in µm	0.0283	11.3	13	43.92

Fig. 2 Weight gain data of modified 9Cr-1Mo steel during air oxidation at 650°C at different durations

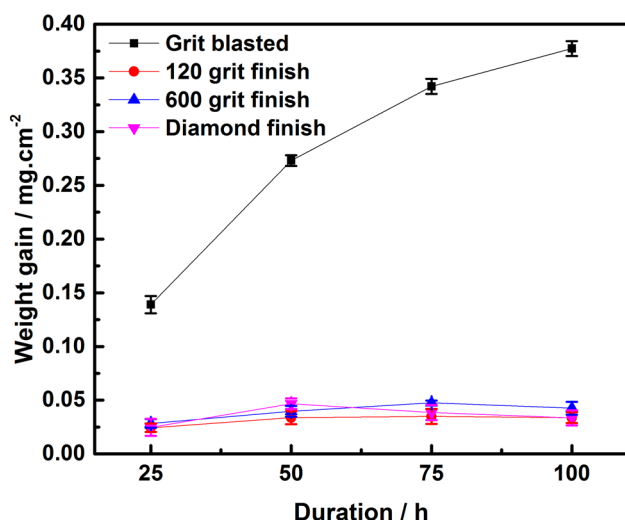**Fig. 3** Squared weight gain versus duration data of modified 9Cr-1Mo steel during air oxidation at 650°C

all other samples, 120 grit, 600 grit and diamond finish, remains more or less constant within the error bars with an increase in the oxidation duration. It is clearly shown the effect of initial surface roughness on the weight gains; as the roughness increases, the gain in weight during oxidation increases. However, the weight gain for 120 grit, 600 grit and diamond finish samples is more or less the same. The weight change is only marginal and is found to increase with the duration of oxidation. Similar observations of more weight gain in the case of grit-blasted sample are observed on Fe-5wt% Al model alloy during air oxidation at 800 and 900 °C for about 24 h duration[15]. The plot of squared weight gain per surface area against duration of oxidation, as shown in Fig. 3, is not linear to the full duration for all the surface finish samples (inset, Fig. 3), indicating the inability of oxidation to follow the parabolic growth kinetics. As seen from Figs. 2 and 3, the oxidation rate observed for the grit-blasted sample is higher compared to the other surface finish samples. The surface roughness of the grit-blasted sample is more, so the real surface area of the sample could be higher than the measured surface, which is used to find out the change in weight per surface area plotted in Figs. 2 and 3. Due to this, the grit-blasted sample shows more weight gain per surface area.

In Fig. 4, the arithmetic mean deviations of the surface roughness profiles (R_a) were plotted for various surface roughness samples. Before oxidation, grit-blasted sample shows more R_a, followed by sample No.2, sample No. 3 and sample No.4. The diamond finish samples (no.4) show a very less R_a value ($R_a = 0.0103$ μm). After the air oxidation, the surface roughness of the samples except for the diamond (mirror) finish sample decrease. The oxides formed will cover the surface roughness to some extent.
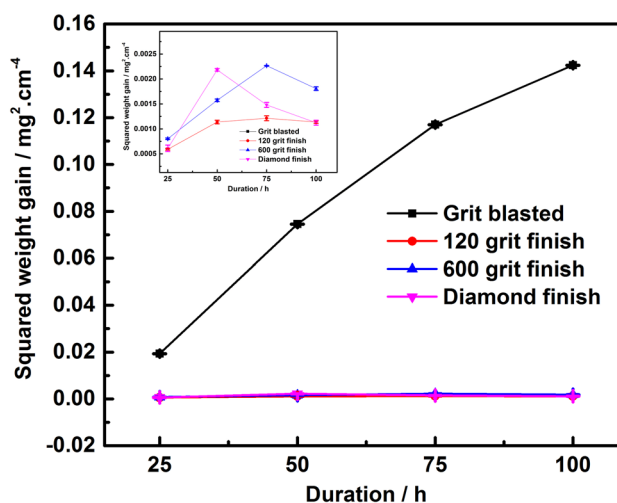
However, in diamond finish sample, the initial surface R_a is insignificant, and hence, the formed oxides surface roughness is higher compared to that before oxidation. The variation in the surface roughness of the samples due to oxidation has occurred and depended on the initial R_a values. The weight gain study shows the dependency of oxidation kinetics or growth of oxide films on the initially finished surface roughness of the sample. As the roughness of the grit-blasted sample is more compared to the diamond, 120 grit finish, and 600 grit finish samples, more surfaces are exposed to the environment leading to more weight gain.
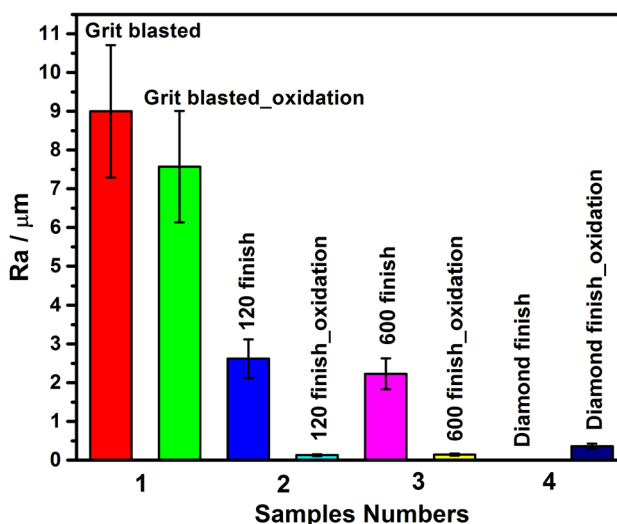

Fig. 4 Arithmetic mean deviation of the surface roughness (R_a) of modified 9Cr-1Mo steel before and after air oxidation at 650°C

3.3 Surface Morphology

Visual observation of the samples after oxidation studies does not show any spallation of the oxide layers. The oxide layers are uniform and are intact to the surface of the sample. The SEM images of the samples after oxidation test for 100 h are provided in Figs. 5 and 6. Figure 5 shows the surface SEM images of grit blasted (Fig. 5a, b) and 120 grit finish samples (Fig. 5c, d). As seen from the figure, the grit-blasted sample surface appears rough after oxidation, and at higher magnification, grains or crystals of grown oxides are seen (Fig. 5b). Since the surface is rougher, the formed oxides could not fully cover the surface heterogeneities, and the oxides exist across the surface within the rough surface. On the other hand, the 120 grit finish sample shows a smooth surface (Fig. 5c) compared to grit-blasted sample with an oxide layer all over the surface (Fig. 5d). In both of the cases, the oxides

Fig. 5 SEM images of the modified 9Cr-1Mo steel specimens after oxidation with different surface treatments for 100 h; **a** & **b**: grit blasted and **c** & **d**: 120 grit finish
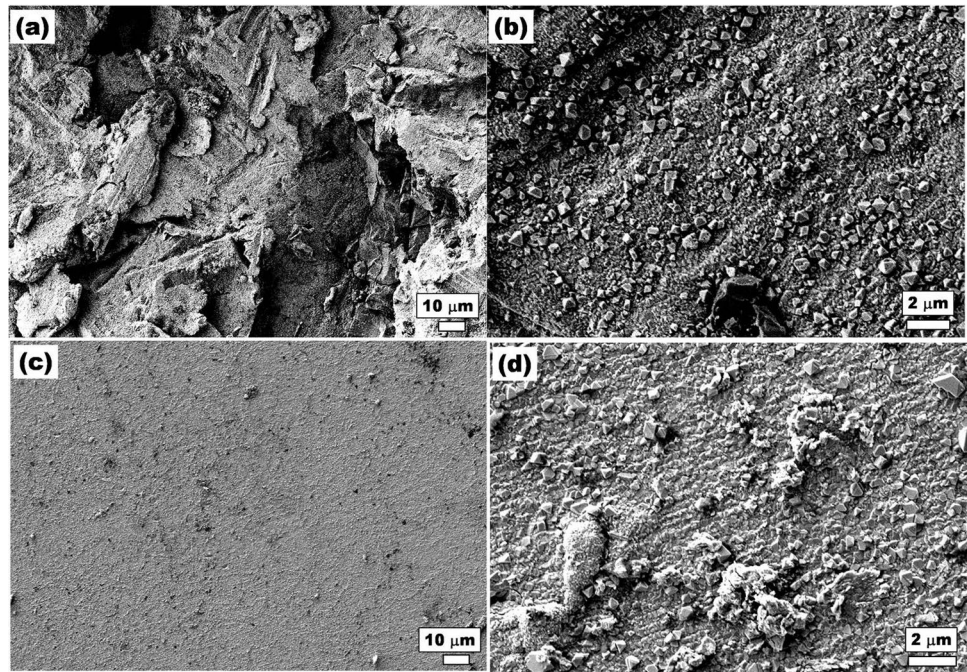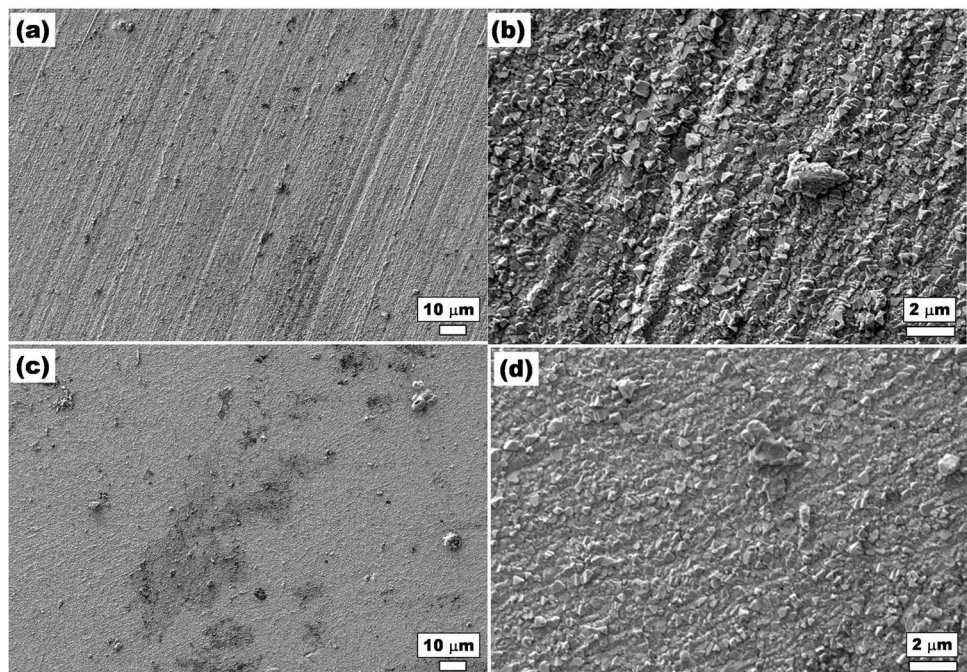

Fig. 6 SEM images of the modified 9Cr-1Mo steel specimens after oxidation with different surface treatments for 100 h; **a** & **b**: 600 grit and **c** & **d**: diamond finish

morphology appears to be similar with spread of oxides in the form of small crystals across the surface.

Figure 6 shows the surface SEM images of the 600 grit finish (Fig. 6a, b) and diamond finish samples (Fig. 6c, d). Both samples show nearly similar surface morphology, with very fine oxide particles grown all over the surface. The oxide layers appear to be rougher (Fig. 6a, b) compared with the oxide layers of diamond finish sample (Fig. 6c, d). This could be due to different surface roughness of the 600 grit and diamond finish samples before oxidation test. The 600 grit sample has more rough surface than the diamond finish sample. After oxidation, the roughness of the 600 grit sample is reduced from its initial roughness due to coverage of the oxide scales; however, the roughness of the diamond finish sample increases due to the formation of oxide particles with rough surfaces. The diamond finish sample after air oxidation shows rougher surface as seen from Fig. 6c, d due to the formation of oxide film composed of small crystals (as seen from Fig. 6d). Hence, the surface roughness measurements showed increase in surface roughness of diamond finish sample from its initial roughness after the air oxidation (Fig. 4).

3.4 Raman Analysis

The Raman spectrum for the samples after 50 h oxidations (Fig. 7) shows the signatures of both hematite and γ-Fe_2O_3. It is clearly observed that the Raman peaks intensity drastically varies with the surface finish of the samples. It indicates that the top most layers of the oxides are mostly comprised of Fe oxides. The Raman spectra of the 100 h oxidized samples are shown in Fig. 8. The Raman spectra
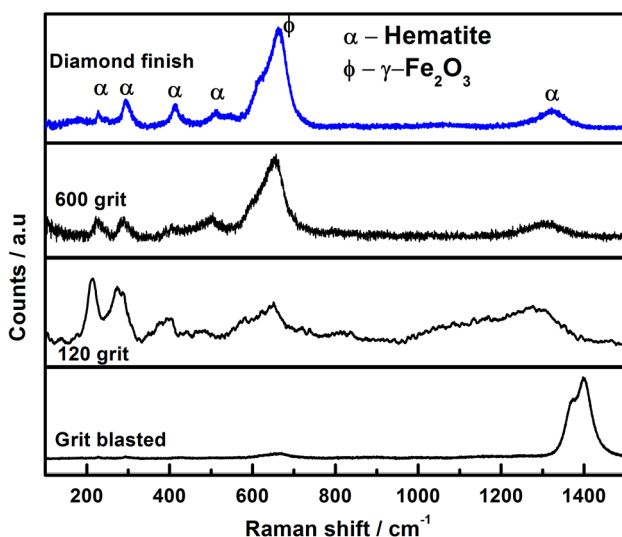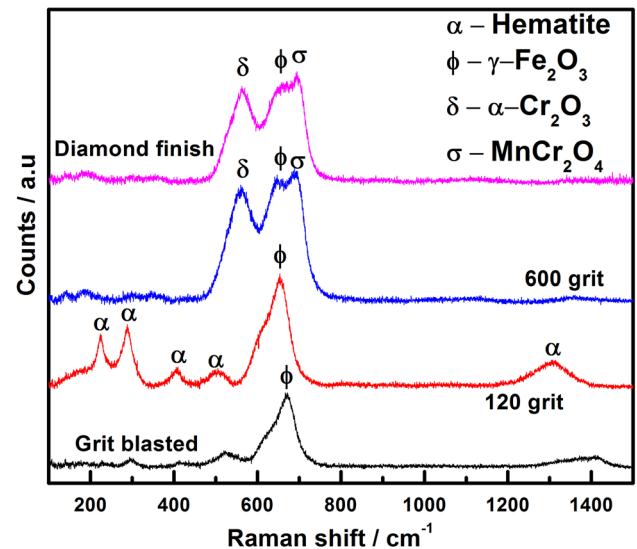

Fig. 8 The Raman spectra of modified 9Cr-1Mo steel with different surface treatments after 100 h of oxidation

of grit blasted sample indicates the presence of γ-Fe_2O_3 and also small intensity peaks corresponding to hematite is found. The air oxidized 120 grit finish sample for 100 h duration shows the presence of both hematite and γ-Fe_2O_3. Both 600 grit finish sample and diamond finish samples showed the presence of $MnCr_2O_4$ and α-Cr_2O_3.

The LRS analysis indicates the existence of Fe- and Cr-rich oxides on the surface of samples along with the presence of $MnCr_2O_4$. Mostly in 9Cr–1Mo steel samples during air oxidation, the formation of Fe–Cr spinels along with Cr_2O_3 and Fe_2O_3 is observed [8, 19, 20]. This observation of the presence of $MnCr_2O_4$ and Cr_2O_3 during LRS analysis for the 600 grit and diamond finish samples generally depends upon the Raman analysis spot on the sample. Since the samples are large and within the analysis spot, those oxides might not be present in the other two samples. However, the presence of Mn-rich oxides is evident on the top surface from the GDOES analysis (Figs. 9, 10).

3.5 GDOES Analysis

The elemental depth profiles of modified 9Cr–1Mo steel after oxidation for 50 h with various surface preparations are shown in Fig. 9. The intense peaks of O and Mn are seen on the top surface followed by Fe and Cr along with O. The oxide films are comprised of Fe, Cr and Mn oxides for all the samples. The outer most layer (top layer) is mostly comprised of Fe-based oxides with Mn oxides, as the Mn peak is seen in all the cases. However, during the Raman analysis, the Mn oxide peaks are not evident. This could be due to the analysis area of the samples. The Raman analysis mostly depends on the spot size and the area in which analysis is

Fig. 7 The Raman spectra of modified 9Cr-1Mo steel with different surface treatments after 50 h of oxidation

Fig. 9 GDOES-DiP profiles of the modified 9Cr-1Mo steel with different surface treatments after 50 h oxidation; **a** Diamond finish **b** 600 grit finish **c** 120 grit finish and **d** Grit blasted samples
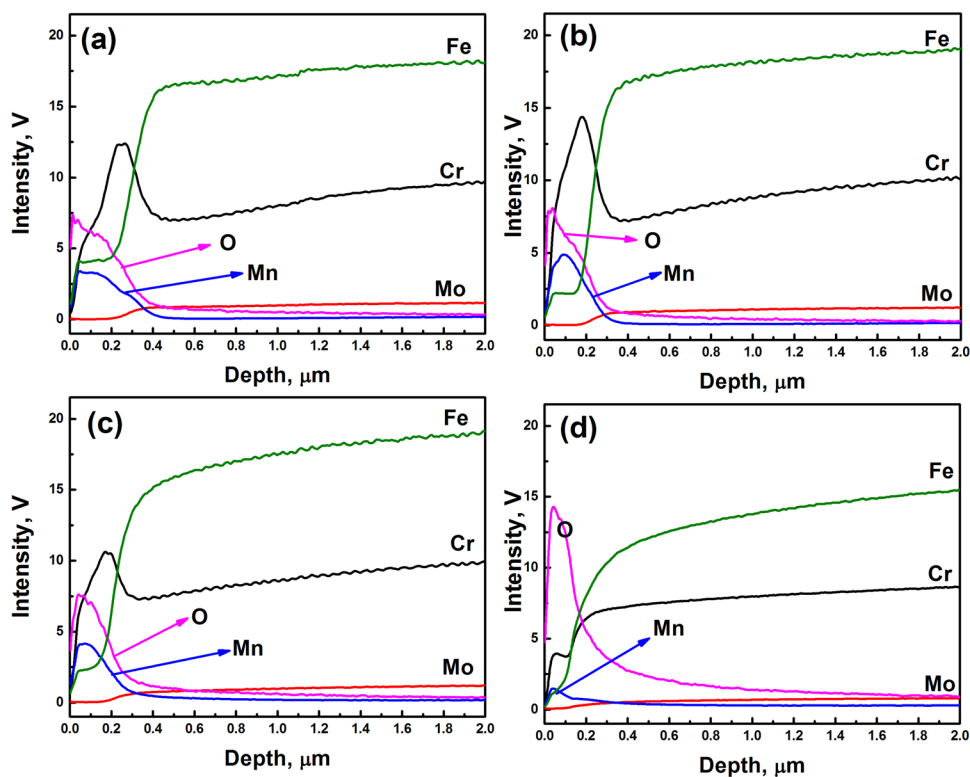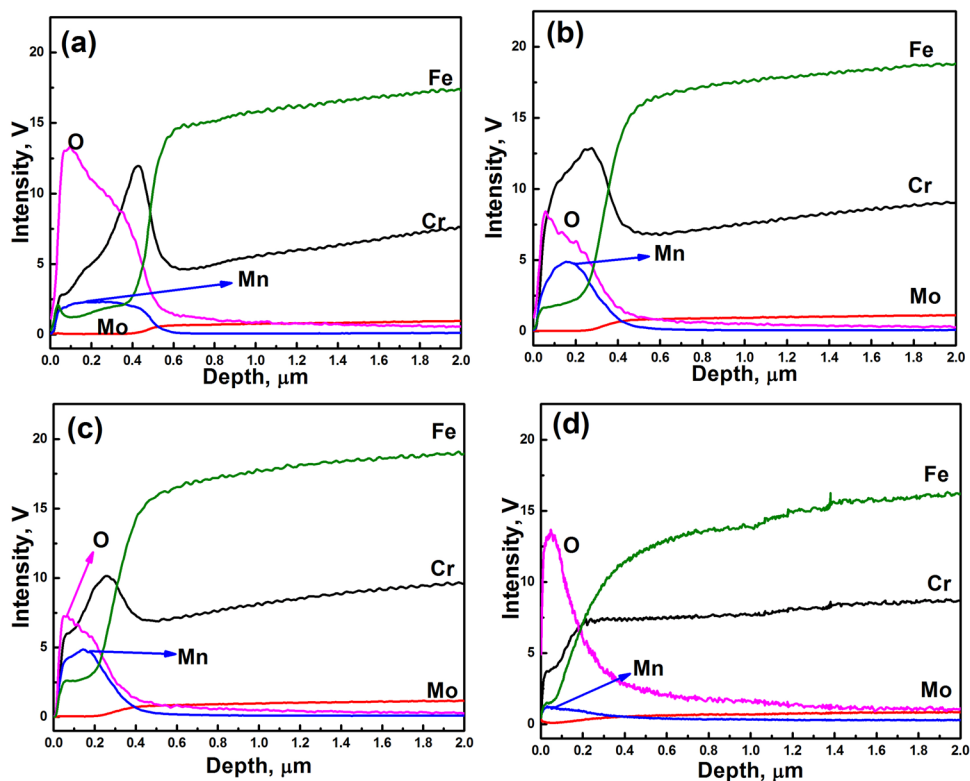

Fig. 10 GDOES-DiP profiles of the modified 9Cr-1Mo steel with different surface treatments after 100 h oxidation; **a** Diamond finish **b** 600 grit finish **c** 120 grit finish and **d** Grit blasted samples

taken. The Raman analysis was done using laser spot size of 3 μm (the analyzed area of the sample is 3 μm), while the GDOES analysis was done using 4 mm dia anode, which sputtered 4 mm dia circular area of the sample. In general, Mn-related oxide formation is not uniform across the surface of the samples after oxidation. The segregation and oxidation

of Mn is observed in modified 9Cr–1Mo during air oxidation [19]. On the other hand, the elemental profile and oxide layer thickness were measured using GDOES technique. The formation of chromium oxides is observed predominantly at the interface of oxide layer and the alloy substrate for all the samples. After the chromium oxides formation at the interface, there is a dip in the concentration of the Cr observed (towards alloy side), which indicates the migration of Cr from the alloy top surface to the oxide layer at the interface. This is observed for all the cases for both studied durations except in grit-blasted sample. This decrease in the concentration of Cr near to the interface would suggest the formation of protective chromium oxide films.

The enrichment of both Cr and Mn is seen from the outer oxide surface (top of oxide layer) to a depth of around 0.300 μm for diamond finish sample, 0.240 μm for 600 grit finish sample, 0.230 μm for 120 grit finish sample and 0.215 μm for grit-blasted sample. The total oxide layer thickness was measured by taking into consideration the decrease in O concentration to half of its maximum peak value, and also half of the value of the increase in Fe intensity [21]. For all the samples, the top oxide layer comprises of Fe, Cr, Mn and O and the intensity of Mo is less compared to the alloy at the top oxide layer, indicating not much Mo-based oxides is formed in the oxide layer.

Similar to the 50 h duration samples, all the samples oxidized for 100 h (Fig. 10) show top oxide layer comprising of Cr, Mn oxides, little amount of Fe seen. The interface between the oxide and alloy is seen with the enrichment of mostly Cr oxides for all the samples except grit-blasted sample. The trend in the intensities of Cr, Mn and O at the top of the oxide layer indicates the formation of $MnCr_2O_4$ spinel as evidenced by the LRS results. The formation of $FeCr_2O_4$ spinel could also be assigned at the interface based on the GDOES profiles as the intensities of Fe, Cr and O seen at the interface. The enrichment of the intensities of the Cr and Mn is found from top of the oxide layer up to a depth of 0.490 μm for diamond finish sample, 0.350 μm for 600 grit finish sample, 0.315 μm for the 120 grit finish sample and 0.300 μm for the grit-blasted sample. Since the grit-blasted sample is more rough, the Mn peak and other features are not clearly resolved in the GDOES analysis.

Figure 11 shows the thickness of the oxide layers on the modified 9Cr–1Mo steel after oxidation studies. The thickness of the oxide film is higher for the diamond finish sample compared to the 600 grit finish, followed by the 120 grit finish and grit-blasted sample. The thickness of the oxide layers for 100 h duration for all the samples found to be higher compared to the 50 h duration. The oxide layer thickness is less in grit-blasted sample even though it shows more weight gain. This could be due to the formation of non-uniform oxide layer on the rough surface.
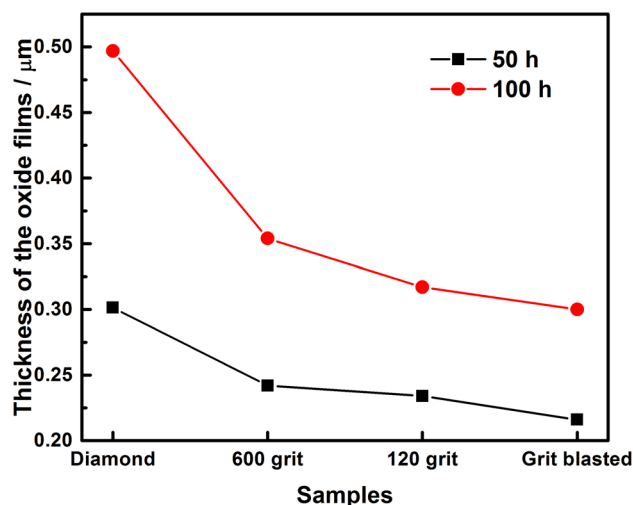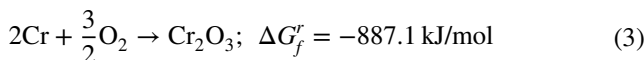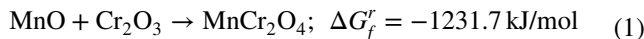

Fig. 11 The thickness of oxide films of modified 9Cr-1Mo steel after air oxidation for different surface treatment samples obtained from GDOES-DiP analysis

The formation of spinel oxides of Mn and Fe with Cr can be understood from the Gibb's energy of formation of the respective reactions at 650 °C as per Eqs. 1 and 2 (calculated using FactSage software version 6.4).

$$MnO + Cr_2O_3 \rightarrow MnCr_2O_4; \ \Delta G_f^r = -1231.7 \, \text{kJ/mol} \quad (1)$$

$$FeO + Cr_2O_3 \rightarrow FeCr_2O_4; \ \Delta G_f^r = -49.4 \, \text{kJ/mol} \quad (2)$$

$$2Cr + \frac{3}{2}O_2 \rightarrow Cr_2O_3; \ \Delta G_f^r = -887.1 \, \text{kJ/mol} \quad (3)$$

The amount of Mn in the 9Cr–1Mo steel is less (0.55 wt%) than Cr (8.97 wt%), and the spinel $MnCr_2O_4$ is not stable as of Cr_2O_3 to protect the underneath alloy. However, the formation of $MnCr_2O_4$ spinel is also favourable as supported by the Gibb's energy of formation. At the interface, the formation of $MnCr_2O_4$ spinel is not evident due to less amount of Mn in the alloy matrix, and since Fe is in more quantity available in the alloy matrix, it reacts with the Cr_2O_3 and forms the corresponding spinel oxides at the interface to some extent. Since the GDOES only provides the presence of Fe to some extent more compared to the top layer at the interface in addition to the enrichment of Cr at the interface, it is believed that both Cr_2O_3 and Fe–Cr spinel might form at the interface.

4 Conclusions

The effect of surface roughness/preparations on the air oxidation behaviour of modified 9Cr–1Mo steel at 650 °C was

studied by applying different surface preparations for about 100 h duration. Four different surface preparations, namely grit blasting, 120 grit finish, 600 grit finish and diamond polishing, were used. The following conclusions could be drawn from the present study:

- The thickness of the oxide layer formed on diamond finish sample was found to be higher compared to the other samples (120 grit finish, 600 grit finish and grit-blasted samples).
- The grit-blasted sample exhibited more weight gain per unit measured surface area among all the samples, but the oxide layer thickness found to be lower.
- The surface roughness of the samples after the air oxidation studies was decreased except for the diamond finish sample, where surface roughness increased.
- The formation of Cr- and Fe-rich oxides on the top surface of oxide layer and also the formation of Cr oxides at the interface were confirmed by the Raman analysis and GDOES measurements. The formation of $MnCr_2O_4$ on the top surface of oxides was also evidenced.
- There is no clear indication of the role of surface finish on the nature of oxides.
- This study indicated the growths of oxide films are higher in the samples with smooth surfaces rather than rough surfaces.

References

1. Mitra T K, Pai A, Kumar P, *Energy Procedia* **7** (2011) 317.
2. Raj B, *Energy Procedia* **7** (2011) 186.
3. Jayakumar T, Mathew M D, Laha K, *Procedia Eng* **55** (2013) 259.
4. Raj B, Mannan S L, Vasudeva Rao P R, Mathew M D, *Sadhana* **27** (2002) 527.
5. Khanna A S, Gnanamoorthy J B, *Oxid Met* **23** (1985) 17.
6. Simms N J, Little J A, *Oxid Met* **27** (1987) 283.
7. Simms N J, Little J A, *Mater Sci Technol* **4** (1988) 1133.
8. Jagadeeswara Ch, Ningshen S, Philip J, *Spectrochim Acta Part B* **172** (2020) 105973.
9. Nowak W J, *J Mater Eng Perform* **29** (2020) 8060.
10. Rai A K, Biswal R, Gupta R K, Rai S K, Singh R, Goutam U K, Ranganathan K, Ganesh P, Kaul R, Bindra K S, *Appl Surf Sci* **495** (2019) 143611.
11. Pour-Ali A, Weiser M, Nguyen N T, Kiani-Rashid A R, *Corros Sci* **163** (2020) 108282.
12. Xia Z X, Zhang C, Huang X F, Liu W B, Yang Z G, *Sci Rep* **5** (2015) 13027.
13. Platt P, Allen V, Fenwick M, Gass M, Preuss M, *Corros Sci* **98** (2015) 1.
14. Ardigo-Besnard M R, Popa I, Heintz O, Chassagnon R, Vilasi M, Herbst F, Girardon P, Chevalier S, *Appl Surf Sci* **412** (2017) 196.
15. Nowak W J, Serafin D, Wierzba B, *J Mater Sci* **54** (2019) 9185.
16. Cheng C Q, Hu Y-B, Cao T-S, Zhang L, Zhu Y-W, Zhao J, *Corros Sci* **176** (2020) 108942.
17. Ghosh S, Kumar M K, Kain V, *Appl Surf Sci* **264** (2013) 312.
18. Das A, Roychowdhury S, Kain V, *J Nucl Mater* **564** (2022) 153672.
19. Swaminathan S, Mallika C, Krishna N G, Thinaharan C, Jayakumar T, Kamachi Mudali U, *Corros Sci* **79** (2014) 59.
20. Khanna A S, Rodriguez P, Gnanamoorthy J B, *Oxid Met* **26** (1986) 171.
21. Shimizu K, Habazaki H, Skeldon P, Thompson G E, Wood G C, *Surf Interface Anal* **27** (1999) 998.